

Application of CFD-DEM method in modeling of wood combustion in a fixed bed

J. K. Tanui¹, P. N. Kioni¹, T. Mirre², M. Nowitzki², D. A. Todorova^{3*}

¹Department of Mechanical Engineering, Dedan Kimathi University of Technology, P.O. Box 657-10100, Nyeri, Kenya

²Department of Engineering and Natural Sciences, Technical University of Applied Science, Wildau, Hochschulring 1, 15745 Wildau, Germany

³Department of Pulp, Paper and Graphic art, University of Chemical Technology and Metallurgy, 8 Kl. Ohridski Blvd., 1756 Sofia, Bulgaria

Received: September 12, 2019; Accepted: May 07, 2020

In this study, a numerical simulation of wood burning in a biomass stove is presented. The main aim was to test the suitability of Computational Fluid Dynamics – Discrete Element Method (CFD-DEM) approach in predicting temperature distribution and species generation in a fixed bed applicable in small-scale biomass stoves. A commercial software code STAR CCM+ was used to simulate combustion of eucalyptus wood under air-fuel condition. Wood burning in a fixed bed was simulated using Lagrange-Euler method, where gas-phase was calculated using computational fluid dynamics while solid-phase was tracked in Lagrange approach. Modeling was validated by comparison with measured data. A good agreement between model and measured data was achieved. Therefore, the CFD-DEM method is a good tool in design and optimization of new combustion equipment.

Keywords: CFD-DEM, Wood combustion, Fixed bed, Temperature distribution

INTRODUCTION

Most people in the world still use small-scale biomass stoves for domestic energy requirements. Biomass combustion significantly contributes to air pollution in terms of particulate matter (PM) or soot and toxic gases [1]. It is a well-known fact that exposure to PM and black carbon from any source causes respiratory and cardiovascular diseases [2]. In addition, some of the pollutants emitted by biomass combustion, for instance, PAH, aldehydes and benzene, are carcinogenic and mutagenic [1]. Therefore, there is need for proper design of biomass burners which have optimum combustion parameters; high efficiency and low emissions.

Biomass conversion to energy is done using different combustion chambers operated under wide conditions. A typical example is a fixed bed combustion chamber. Biomass combustion in a fixed bed is affected by fuel type and composition, air flow rate, amount of moisture in the fuel, fuel shape and size [3, 4]. These factors also affect emission characteristics of the fixed bed reactor. Careful consideration of these factors should be taken into account when designing a biomass burner.

CFD is an important tool in designing and optimization of new burner equipment, as well as troubleshooting old devices. It helps in understanding combustion processes which take place in a burner. CFD simulations give an approximate of these physical and chemical processes. However, they do not give a detailed

description of all the relevant combustion phenomena. Modeling of biomass thermal conversion in a packed bed have been differently approached. Using one-dimensional models, different researchers [5–7] have studied the propagation of ignition front and the reactions in a fixed bed of biomass fuels. These models do not consider individual particles, hence they do not accurately predict thermal conversion of fixed bed and require an experimentally determined empirical correlation. Another approach is the single particle model, where conversion of packed bed is constituted by summation of individual particle conversion. Through this approach the effects of initial relative velocity, free stream oxygen concentration, particle size, pre-exponential factor and particle entrainment on the conversion of a single particle have been investigated [8–10]. Recently, three-dimensional models for simulating combustion in a fixed bed have been developed [11–13]. Collazo *et al.* [11] simulated a fixed bed reaction using a 3D model that did not consider bed shrinkage. A 3D model that considers bed movement was developed by Mahmoudi *et al.* [14]. In this model, gas phase was modeled as three-dimensional, while solid phase was modeled as one-dimensional. Although an extensive CFD research has been done on fixed bed combustion, a few researchers use detailed models to predict both bed and freeboard biomass combustion in a fixed bed.

* To whom all correspondence should be sent:

E-mail: todorova.dimitrina@uctm.edu

The main aim of this study was to test the suitability of the CFD-DEM approach in predicting temperature distribution and species generation in a fixed bed. Experimental tests were carried out in a laboratory-scale fixed bed. Temperature distribution in the bed was measured and compared to CFD-DEM results.

EXPERIMENTAL

A schematic diagram and a photo of the experimental set-up used in this work are shown in Fig. 1. A detailed description of the set-up has been given in our previous paper [15]. It is a cylindrical chamber with an internal diameter of 40 mm and a height of 200 mm. Air inlet port is located at the bottom and grate is located 40 mm from it. Flue gas

outlet is located at the top of the chamber. Wood particles were fed up to a height of 6 cm.

Proximate and ultimate analysis for the wood samples investigated in this study are presented in Table 1 and physical properties - in Table 2.

Numerical simulations of combustion of wood in a fixed bed were carried out using a commercial software CD-Adapco (STAR CCM+ version 11.04) [16]. Wood burning in a fixed bed was simulated using Lagrange-Euler method, where gas-phase was calculated using computational fluid dynamics (Euler phase) while solid-phase was tracked in Lagrange phase (discrete element method). A detailed description of the governing equations is given in Ref. [16].

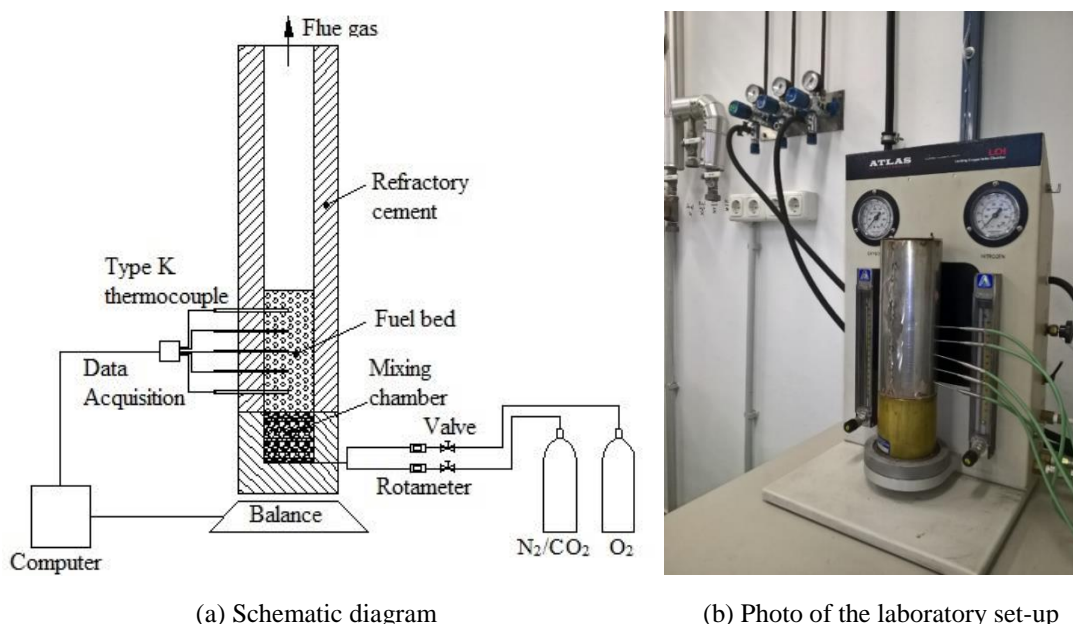


Figure 1. Experimental set-up.

Table 1. Proximate and ultimate analysis of fuel sample.

Proximate Analysis	(wt %)	Standards
Moisture	10.3	CEN-TS 14774-2:2009
Volatile matter (wt% dry basis)	84.9	CEN-TS 15148:2009
Fixed carbon (wt% dry basis) - by difference	14.9	-
Ash (wt% dry basis)	0.2	CEN-TS 14775:2009
Ultimate Analysis	(wt % dry basis)	Standards
C	50.87	CEN-TS 15104:2011
H	5.73	CEN-TS 15104:2011
N	0.3	CEN-TS 15104:2011
O (by difference)	43.1	-
Gross calorific value (MJ/kg)	19.3	CEN-TS 14918:2009

Table 2. Physical properties of wood

Particle diameter, d_p (m)	0.005
Eucalyptus wood	
Density, ρ (kg/m ³)	1220
Porosity, θ	0.64
Specific heat, c_p (J/kgK)	$1500 + T_s$
Conductivity, λ_s (W/mK)	0.2
Char	
Density, ρ (kg/m ³)	250
Porosity, θ	0.85
Specific heat, c_p (J/kgK)	$420 + 2.09T_s - 6.85 \times 10^{-4} T_s^2$
Conductivity, λ_s (W/mK)	0.1

The geometrical configuration of the combustion chamber shown in Fig. 1 was meshed into a highly-refined unstructured grid. The computational mesh consisted of approximately 200,000 cells.

Chemical kinetics of wood conversion in the bed was simulated using different sub-models, which consisted of drying model, pyrolysis model, homogeneous reaction model and char oxidation and gasification model. Kinetic data of these sub-models are given in Table 3.

The cold air at a temperature of 295 K enters the burner through the bottom boundary modeled as mass flow boundary, and hot combustion products exit the domain through the top boundary modeled as pressure outlet boundary. The air flow rate at the inlet was 0.1 kg/m²s while the mass fractions concentration of O₂ and N₂ were specified using the standard air composition. A stationary wall with no-slip conditions was considered; the tangential velocity at the wall was explicitly set to zero. Heat transfer by radiation and convection at the wall were considered. Emissivity of the surface and coefficient of heat transfer were assumed to be 0.8 and 10 W/m² K, respectively.

RESULTS AND DISCUSSION

The model results were validated by comparing predicted and measured temperature at corresponding positions in the fuel bed. Shown in Fig. 2 is the temperature history at 5 cm from bed bottom. A good agreement between predicted and measured temperature values is achieved. The graph shows that the temperature profile has two peaks; the first peak is about 1200 K while the second peak is about 1400 K. As the flame front passes the position where measurement is done, temperature rises rapidly up to the first peak. Then it gradually

decreases to about 900 K where it starts to rise again. This phase of combustion is characterized by both exothermic and endothermic processes. Exothermic reactions of the volatiles increase the temperature while drying and pyrolysis, which are endothermic processes, decrease the temperature. The second part of the graph, where temperature rises, signifies the end of endothermic processes. The volatiles transported from the lower part of the bed burn in this phase. The last regime, where temperature decreases, is characterized by char gasification and oxidation. Whereas char oxidation increases the temperature, char gasification with H₂O and CO₂ decrease the temperature. Overall decrease in temperature indicates that gasification is the dominant process in this regime.

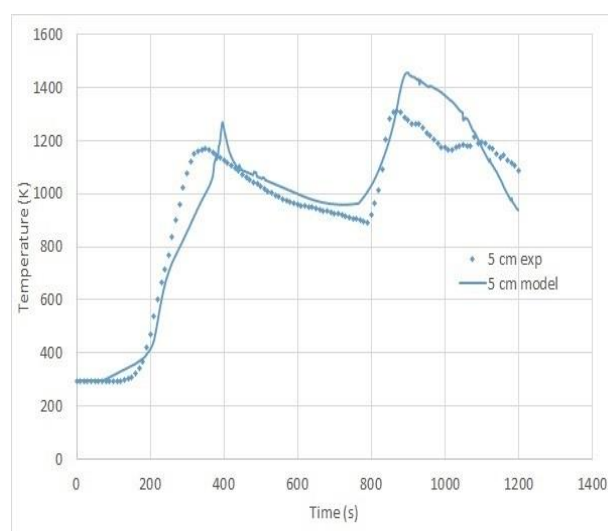


Figure 2. Measured and predicted temperature profile at 5 cm from fuel bottom.

Presented in Fig. 3 are the gas-phase and particle surface temperatures at different times. The figures clearly reveal the movement of reaction front from top to bottom as combustion proceeds. Temperature distribution at the same cross-section is non-uniform. Some particles have higher temperature than others located within the same height. Particles close to the wall have higher temperatures compared to corresponding particles close to the centre. This is because walls were modeled in such a way that small amount of heat is lost.

Initially, the bed is ignited at the top. During ignition, a lot of heat is absorbed by the particles. This heat is used for drying and pyrolysis which occur simultaneously, and the bed temperature does not significantly increase, as illustrated in Figs. 3(a) and (b). Once pyrolysis products are released, they react with O₂ and release more heat which increases the temperature, as shown in Fig. 3(c).

Table 3. Biomass kinetic model

Drying		Rate expression	Source
R(1)	Wet wood \rightarrow Dry wood + H ₂ O (g)	$R_{dry} = Y_{mp,b,wet} 1.6 \times 10^{27} \exp(-25000/T_s)$	[17]
Pyrolysis Reactions			
		Rate expression, Kinetics:	Source
		$K_i = A_i T^n \exp(-E_i/RT)$	
R(2)	Dry wood \rightarrow gas	$w'_b = K_2 \rho_{b,dry}$	[18]
R(3)	Dry wood \rightarrow tar	$w'_b = K_3 \rho_{b,dry}$	[18]
R(4)	Dry wood \rightarrow char	$w'_b = K_4 \rho_{b,dry}$	[18]
R(5)	Tar $\rightarrow \gamma_t \text{Tar}_{inert} + \gamma_{CO} \text{CO} + \gamma_{CO_2} \text{CO}_2 + \gamma_{H_2} \text{H}_2 + \gamma_{CH_4} \text{CH}_4$	$w'_{tar} = K_5 \rho_{tar}$	[13, 14]
Homogeneous Gas-Phase Reactions			
		Rate expression, Kinetics:	Source
		$K_i = A_i T^n \exp(-E_i/RT)$	
R(6)	$2\text{CO} + \text{O}_2 \rightarrow 2\text{CO}_2$	$R_{CO} = K_6 [\text{CO}] [\text{O}_2]^{0.25} [\text{H}_2\text{O}]^{0.5}$	[13, 14]
R(7)	$\text{CH}_4 + 2\text{O}_2 \rightarrow \text{CO}_2 + 2\text{H}_2\text{O}$	$R_{CH_4} = K_7 [\text{CH}_4]^{0.7} [\text{O}_2]^{0.8}$	[13, 14]
R(8)	$2\text{H}_2 + \text{O}_2 \rightarrow 2\text{H}_2\text{O}$	$R_{H_2} = K_8 [\text{H}_2] [\text{O}_2]$	[13, 14]
R(9)	$\text{Tar} + 2.9\text{O}_2 \rightarrow 6\text{CO} + 3.1\text{H}_2$	$R_{tar} = K_9 [\text{Tar}]^{0.5} [\text{O}_2]$	[13, 14]
R(10)	$\text{CO} + \text{OH} \rightarrow \text{CO}_2 + \text{H}$	$R_{CO} = K_{10} [\text{CO}] [\text{OH}]$	[19]
R(11)	$\text{H} + \text{O}_2 \rightarrow \text{O} + \text{OH}$	$R_H = K_{11} [\text{O}] [\text{OH}]$	[19]
R(12)	$\text{H}_2 + \text{O}_2 \rightarrow \text{OH} + \text{OH}$	$R_{H_2} = K_{12} [\text{H}_2] [\text{O}_2]$	[20]
R(13)	$\text{H}_2\text{O} + \text{CO} \rightarrow \text{CO}_2 + \text{H}_2$	$R_{H_2O} = K_{13} [\text{H}_2\text{O}] [\text{CO}]$	[17, 18]
R(14)	$\text{CO}_2 + \text{H}_2 \rightarrow \text{H}_2\text{O} + \text{CO}$	$R_{CO_2} = K_{14} [\text{CO}_2] [\text{H}_2]$	[17, 18]
Heterogeneous Reactions			
		Rate expression, Kinetics:	Source
		$K_i = A_i T^n \exp(-E_i/RT)$	
R(15)	$\Omega \text{C} + \text{O}_2 \rightarrow 2(\Omega - 1) \text{CO} (2 - \Omega) \text{CO}_2$	$w'_{char,oz} = K_{15} P_{O_2} S_{a,char}$	[13, 14]
R(16)	$\text{C} + \text{CO}_2 \rightarrow 2\text{CO}$	$w'_{char,CO_2} = K_{16} P_{CO_2} S_{a,char}$	[13, 14]
R(17)	$\text{C} + \text{H}_2\text{O} \rightarrow \text{CO} + \text{H}_2$	$w'_{char,H_2O} = K_{17} P_{H_2O} S_{a,char}$	[13, 14]

Heat spreads to other particles by radiation, convection and conduction. As the reaction front moves downward, more pyrolysis products are released. These products are not completely reacted at their point of production. Some are transported downstream (freeboard region) where they react and generate more heat which significantly increases the temperature, as shown in Figs. 3 (d) and (e). After the reaction front moves from top to bottom, all particles in fuel bed have undergone devolatilization. As a result, the fuel bed has slightly shrunk, as shown in Fig. 3(f). The remaining biomass is now pure char which is undergoing heterogeneous reactions with O_2 , H_2O and CO_2 . The overall temperature decreases because char endothermic reactions with H_2O and CO_2 are dominant in this phase. It is also noted that in the vicinity of the grate, temperatures are lower than in the other region of the bed. Convective cooling due to cold air inlet causes this effect.

Illustrated in Figs. 4 and 5 is the mass fraction distribution of the major combustible species of pyrolysis; tar and CO. Likewise to temperature distribution, the species mass fraction distribution at a given cross-section is also non-uniform. Nonetheless, the flame front propagation is clearly depicted. Significant amounts of tar and CO are produced in the fuel bed from ignition up to about 750 s, as shown in Figs. 4 and 5. During this period, devolatilization is the dominant process. At 1000 s,

Figs. 4 and 5, traces of the volatiles noticeable in the bed indicate a char combustion stage.

Volatiles released from the bed burn within or outside the bed. The tested flow rate of oxidant is high enough to oxidize all the volatiles, as shown in Fig. 6. As the flame front moves downward, the amount of tar and CO released at its position decrease. This could be attributed to non-uniformity of flame front movement. Some particles at the same level get heated and pyrolyzed faster than others.

Shown in Fig. 7 is water vapor (H_2O) mass fraction distribution in the fuel bed. H_2O is a gaseous product arising from particle evaporation. It is also one of the pyrolysis products. In addition, H_2O in the bed is due to oxidation of CH_4 and H_2 . During initial stages of combustion, for instance, ignition up to 300 s, most of H_2O is confined to the fuel bed. This is because during this period H_2O is mostly from particle evaporation and pyrolysis. As combustion proceeds, e.g. from 400 s to 1000 s, H_2O generated in the fuel bed is spread to freeboard region by convection. It is important to notice that at this time, all the aforementioned sources participate in its production making it more pronounced than at the earlier stage. H_2O together with CO_2 are the main products of combustion that radiate heat. As a result, their effect on temperature distribution is seen in Fig. 3.

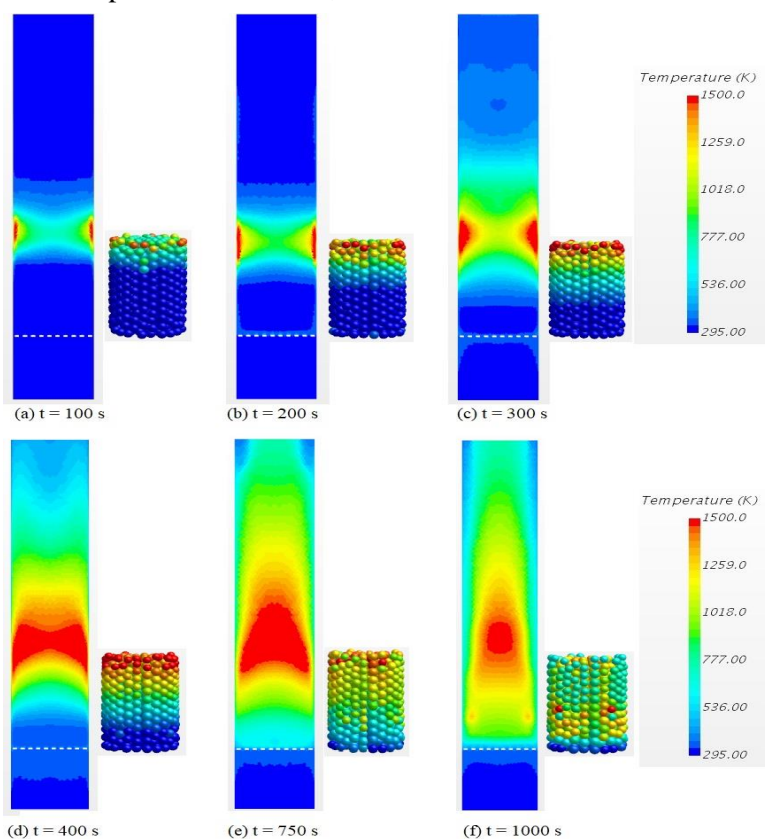


Figure 3. Gas-phase and particle surface temperature distribution in the wood fuel bed at different times.

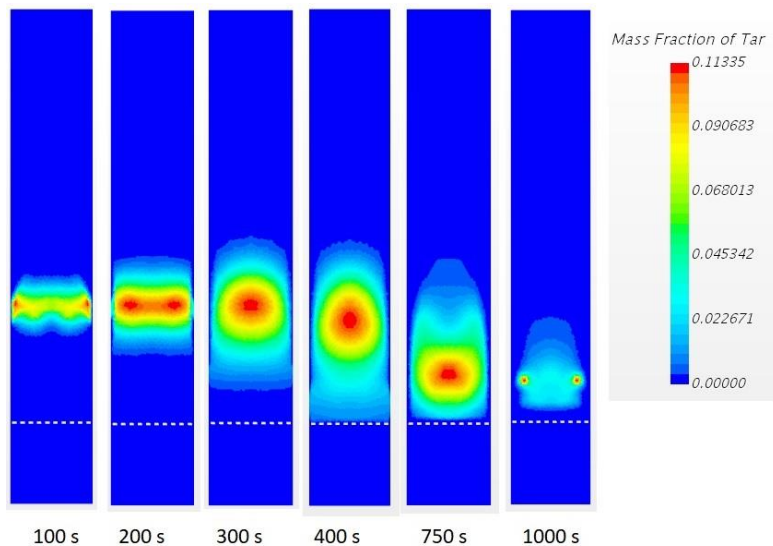


Figure 4. Tar mass fraction distribution in the wood fuel bed burning at 21%O₂/79%N₂ at different times.

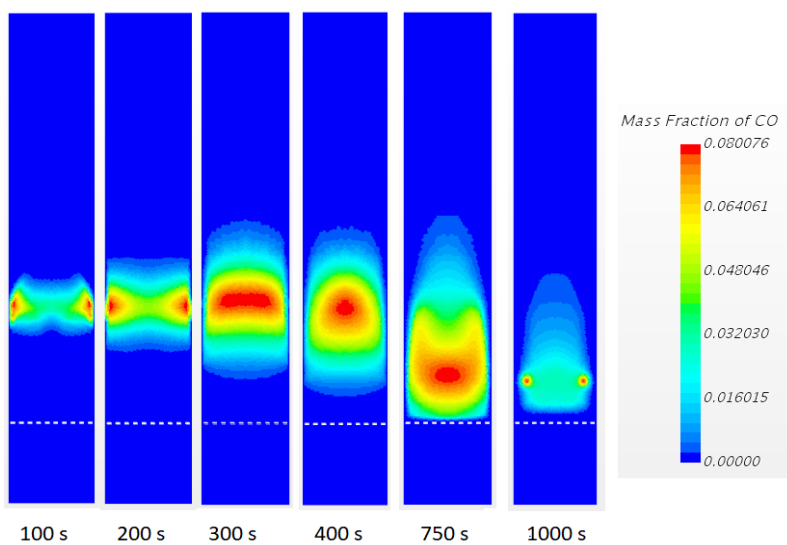


Figure 5. CO mass fraction distribution in the wood fuel bed burning at 21%O₂/79%N₂ at different times.

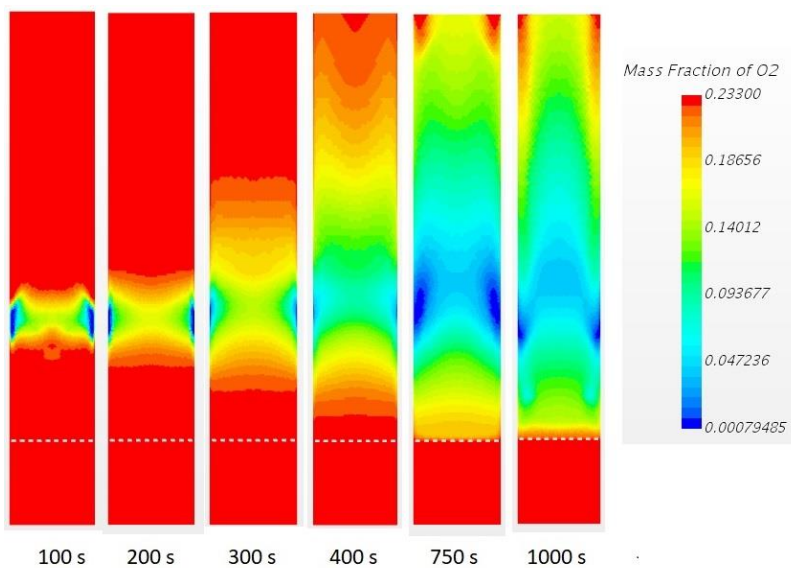


Figure 6. O₂ mass fraction distribution in the wood fuel bed burning at 21%O₂/79%N₂ at different times.

Presented in Fig. 8 is the mass fraction distribution of CO₂ in the burner. CO₂ is a product which arises from pyrolysis, as well as oxidation of CO, CH₄ and char. Its production is also contributed by tar cracking reaction. During the initial stage of combustion, 100 s to 300 s, it is observed that CO₂ production is minimal and restricted to the fuel bed. CO₂ generation is more pronounced in the last stage of combustion, 750 s and 1000 s. This is char combustion stage where char is oxidized into CO and CO₂ which increases its amount in the burner. The role of CO₂ in temperature distribution through radiation is also seen in Fig. 3.

Flame structures at different positions from fuel bed bottom are presented in Fig. 9. The graphs show

that in the freeboard region flame structures at different positions have similar profiles but differ in magnitude. Since the fixed bed that was tested was operated in batch mode under unsteady conditions, the amount of heat released changed with respect to time. At 10 cm, intense heat is released between 170 s and 600 s, while at 15 cm it is at 200 s to 600 s. These periods fall within the devolatilization stage where volatiles transported to these positions react and generate heat. Temperature then gradually decreases until the end of combustion. During this time, heat present in these positions is due to convection and radiation from fuel bed.

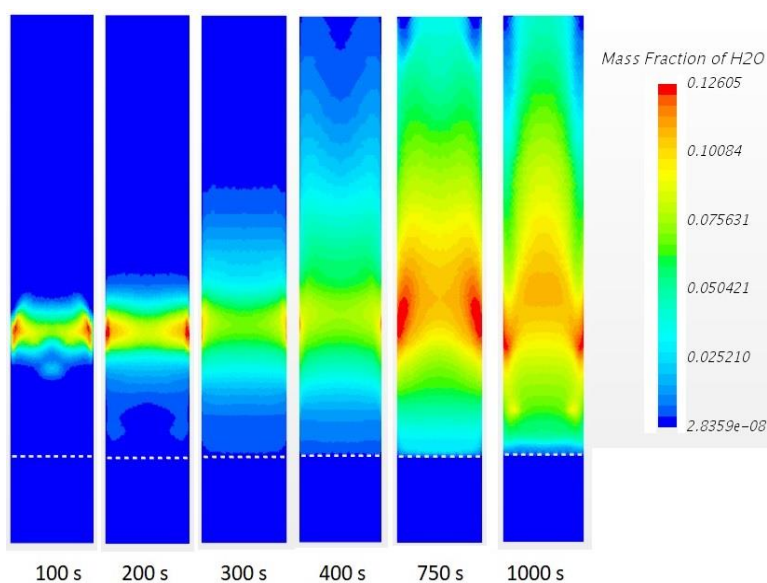


Figure 7. H₂O mass fraction distribution in the wood fuel bed burning at 21%O₂/79%N₂ at different times.

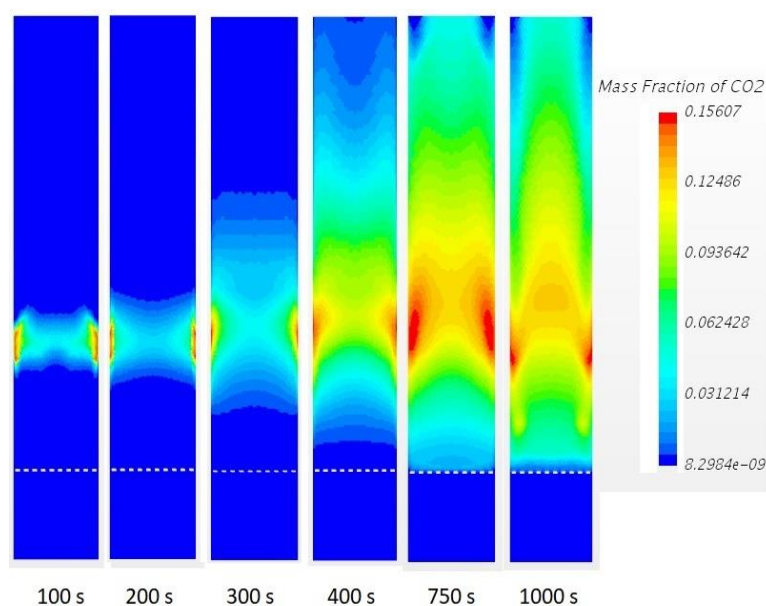


Figure 8. CO₂ mass fraction distribution in the wood fuel bed burning at 21%O₂/79%N₂ at different times.

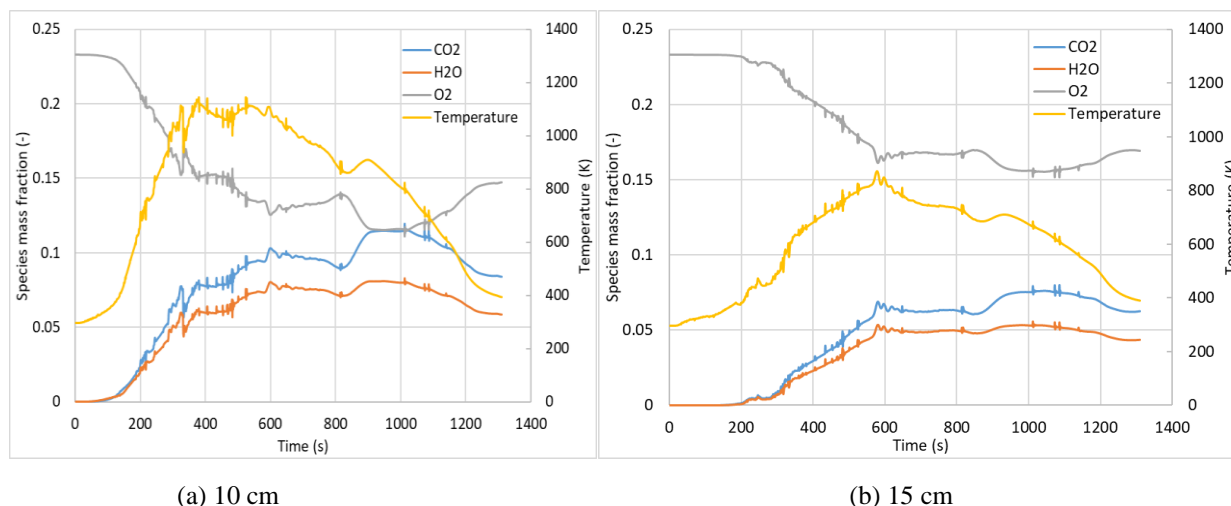


Figure 9. Major species and temperature profiles at different positions from fuel bed bottom for wood combustion at 21% O₂/79% N₂.

CONCLUSION

This study presented modeling of fixed bed combustion of wood using the CFD-DEM approach. The modeling results were validated with measurements done in a laboratory-scaled fixed bed. A good agreement between model and experimental results was achieved. Temperature distribution at the same cross-section is non-uniform. Some particles have higher temperature than others located within the same height. Likewise, species mass fraction distribution at a given cross-section is also non-uniform. Nonetheless, the flame front propagation is clearly depicted. In the freeboard region, flame structures at different positions have similar profiles but differ in magnitude. Therefore, it was proven that CFD-DEM is a good tool in design, optimization and analysis of fixed bed furnaces.

Acknowledgement: This work was financially supported by both Dedan Kimathi University of Technology, Kenya and Technical University of Applied Science Wildau, Germany. The first author would like to thank the German Academic Exchange Service (DAAD) for granting him stipend while undertaking this work at the Technical University of Applied Science, Wildau, Germany.

REFERENCES

1. S. Jiménez, J. Ballester, *Proc. Combust. Inst.*, **30**, 2965 (2005).
2. S. Jiménez, J. Ballester, *Combust. Flame*, **140**, 346 (2005).
3. Y. Bin Yang, C. Ryu, A. Khor, V. N. Sharifi, J. Swithenbank, *Fuel*, **84**, 2026 (2005).
4. S. Mahapatra, S. Dasappa, *Fuel Process. Technol.*, **121**, 83 (2014).
5. M. Fatehi, M. Kaviany, *Combust. Flame*, **99**, 1 (1994).
6. J. J. Saastamoinen, R. Taipale, *Combust. Flame*, **123**, 214 (2000).
7. S. Kumar, S. Dasappa, *Appl. Therm. Eng.*, **112**, 1382 (2017).
8. B. Peters, *Combust. Flame*, **146**, 132 (2002).
9. J. C. Lee, R. A. Yetter, F. L. Dryer, *Combust. Flame*, **101**, 387 (1995).
10. M. Y. Ha, B. R. Choi, *Combust. Flame*, **97**, 1 (1994).
11. J. Collazo, J. Porteiro, D. Patiño, E. Granada, *Fuel*, **93**, 149 (2012).
12. A. H. Mahmoudi, F. Hoffmann, B. Peters, *Appl. Therm. Eng.*, **93**, 1091 (2016).
13. A. H. Mahmoudi, F. Hoffmann, M. Markovic, B. Peters, G. Brem, *Combust. Flame*, **163**, 358 (2016).
14. A. H. Mahmoudi, M. Markovic, B. Peters, G. Brem, *Fuel*, **150**, 573 (2015).
15. J. K. Tanui, P. N. Kioni, T. Mirre, M. Nowitzki, *Fuel Process. Technol.*, **179**, 285 (2018).
16. CD-Adapco, "STAR CCM+ Version 11.04," www.cd-adapco.com, 2017.
17. R. Johansson, H. Thunman, B. Leckner, *Combust. Flame*, **149**, 49 (2007).
18. M. A. Gómez, J. Porteiro, D. de la Cuesta, D. Patiño, J. L. Míguez, *Fuel*, **184**, 987 (2016).
19. G. P. Smith, D. M. Golden, M. Frenklach, N. W. Moriarty, B. Eiteneer et al., "GRI-Mech 3.0," 1999. <http://combustion.berkeley.edu/gri-mech/version30/text30.html>.
20. C. K. Westbrook, F. L. Dryer, *Prog. Energy Combust. Sci.*, **10**, 1 (1984).